

Article

Groundwater Tracer Tests as a Supporting Method for Interpreting the Complex Hydrogeological Environment of the Urbas Landslide in NW Slovenia

Luka Serianz * and Mitja Janža 

Geological Survey of Slovenia, Dimičeva ulica 14, 1000 Ljubljana, Slovenia; mitja.janza@geo-zs.si

* Correspondence: luka.serianz@geo-zs.si

Abstract: This study investigates groundwater flow patterns in a landslide area above the settlement of Koroška Bela in NW Slovenia using a series of tracer tests with sodium chloride (NaCl) and fluorescein (uranine). The tracer experiments, using a combination of pumping tests and continuous groundwater observations, reveal two distinct groundwater flow horizons within the landslide body: a prevailing shallower flow within highly permeable gravel layers and a slower deep flow in the weathered low-permeability clastic layers. Uranine injections suggest longer retentions, indicating complex hydrogeological conditions. Groundwater is recharged by the infiltration of precipitation and subsurface inflow from the upper-lying carbonate rocks. In the upper landslide, highly permeable gravel layers accelerate flow, especially during heavy rainfall, while downstream interactions between permeable gravel and less permeable clastic materials create local aquifers and springs. These groundwater dynamics significantly influence landslide stability, as rapid infiltration during intense precipitation events can lead to transient increases in pore water pressure, reducing shear strength and potentially triggering slope movement. Meanwhile, slow deep flows contribute to prolonged saturation of critical failure surfaces, which may weaken the landslide structure over time. The study emphasizes the region's geological heterogeneity and landslide stability, providing valuable insights into the groundwater dynamics of this challenging environment. By integrating hydrogeological assessments with engineering measures, the study provides supportive information for mitigating landslide risks and improving groundwater management strategies.



Academic Editor: Cheng-Yu Ku

Received: 30 January 2025

Revised: 23 February 2025

Accepted: 27 February 2025

Published: 3 March 2025

Citation: Serianz, L.; Janža, M. Groundwater Tracer Tests as a Supporting Method for Interpreting the Complex Hydrogeological Environment of the Urbas Landslide in NW Slovenia. *Appl. Sci.* **2025**, *15*, 2707. <https://doi.org/10.3390/app15052707>

Copyright: © 2025 by the authors. Licensee MDPI, Basel, Switzerland. This article is an open access article distributed under the terms and conditions of the Creative Commons Attribution (CC BY) license (<https://creativecommons.org/licenses/by/4.0/>).

Keywords: groundwater; tracer; landslide; Carboniferous and Permian clastic rocks

1. Introduction

Landslides are one of the most common natural hazards in mountainous regions, including the Alps, posing significant threats to infrastructure and human lives. A major trigger of shallow landslides on steep terrain is heavy rainfall, which often leads to a rapid increase in pore water pressure as well as groundwater-level rise, thus (re)activating slope movements [1–5]. Several studies emphasize the important role of the underlying bedrock, which can play a key role in runoff on steep terrain [6–9]. Therefore, it is crucial to understand to what extent the bedrock is connected to soil structures. This is especially important in predicting the changes in pore water pressure in slopes, which can be used to forecast shallow landslides [10].

Given the complexity of landslide processes, researchers rely on various research methods to understand the dynamics of these processes more thoroughly. Among these methods, tracer tests could serve as an essential tool in interpreting the movement of

water within landslides. Groundwater tracer tests are often used for hydrogeological characterization of groundwater flow [11], particularly in karst aquifers [12–16]. In the context of landslides, tracer tests help to track particles and fluids as they move through the landslide material, providing insight into the internal processes at work, such as groundwater movement and sediment transport, as well as the formation of forces. These tests are particularly valuable for predicting landslide behavior and improving risk models in landslide-prone regions.

To our knowledge, there are only a few studies that have applied tracer tests in landslides, as they can be logistically complex and expensive [17]. The studies were conducted either to define rainfall infiltration processes [18,19] or to define groundwater flow paths and their velocities (e.g., [17,20–24]). According to [21], tracer experiments in landslides are mainly interpreted semi-quantitatively or qualitatively in order to assess local groundwater flow paths and verify hydraulic connections between different parts of a landslide body.

Tracer tests were used in this study to determine the groundwater flow paths in the area of the Urbas landslide and its recharge characteristics. Several site investigations and monitoring projects have been carried out in recent years, which have helped to improve our knowledge about the landslide [25–29]. Recent studies on hydrogeological conditions have focused on stable isotopes, which were used to assess the main groundwater flow components and their residence times [30].

Three series of tracer tests were carried out for this study: the first in spring 2020, the second in autumn 2020, and the last in spring 2022. Both uranium (fluorescein) and sodium chloride were injected into the first two series of tests, while only fluorescein was used in the last campaign. The fluorescent tracers were selected for their high detection sensitivity, low cost, and low toxicity [31]. To improve the hydrogeological conceptual model of the landslide, the results of a pumping test carried out in 2020 and the data from continuous hydrogeological monitoring were also included.

2. Case Study

The Urbas landslide is located in the Potoška Planina area, NW Slovenia, on the southern slopes of the Belščica and Stol peaks in the Karavanke mountain range (Figure 1). The landslide covers an area of 177,000 m² [26], with steep slopes (generally from 30 to 70°) at altitudes of 1200 m to 1350 m (Figure 1). The volume of the sliding mass was estimated at 1,578,700 m³ [26]. It is a source area for debris flow and poses a risk to the settlement of Koroška Bela [29]. The sliding mass consists of tectonically deformed and weathered Upper Carboniferous-to-Permian claystone, siltstone, sandstone, conglomerate, and carbonate rocks covered by talus material from upper-lying Triassic-to-Lower Jurassic carbonate rocks [26,32,33]. The landslide is a deep-seated rotational slide with a main sliding surface at a depth of approx. 15 m, with surface displacements of 6 cm in the upper part and 40 cm in the lower part [28].

The average annual precipitation in the area is 1950 mm, with peaks in autumn and spring [34]. Snow cover is present for some 110 days per year [35,36], and the average annual temperature is 4–6 °C [37].

The groundwater in the landslide is recharged by the infiltration of precipitation and subsurface inflow from the karst-fissured aquifers in the carbonate rocks that form the upper part of the landslide recharge area [30]. Below the steep limestone ridge, scree and rockfall (talus) material accumulates and covers the upper part of the landslide [38]. The groundwater level and thickness of the saturated zone in this material depends primarily on the morphology of the upper boundary of the low-permeability Paleozoic clastic and carbonate rocks. The main surface water spring is Urbas, located in the middle part of

the landslide. The observed discharge of the spring is between 0.7 L/s and 20 L/s [25]. After heavy rainfall, these values are likely to be exceeded. The water from the spring is used for the water supply of the mountain huts in the vicinity. Some additional springs and marshes are linked to contacts between the low-permeability landslide body and the overlying limestone debris. The precipitation distribution in the region is influenced by elevation and slope exposure in the Julian Alps and Karavanks. The estimated average recharge altitude of springs originating at the landslide ranges from approximately 1700 to 1800 m a.s.l., with mean residence times ranging from 2 to 5 months [30].

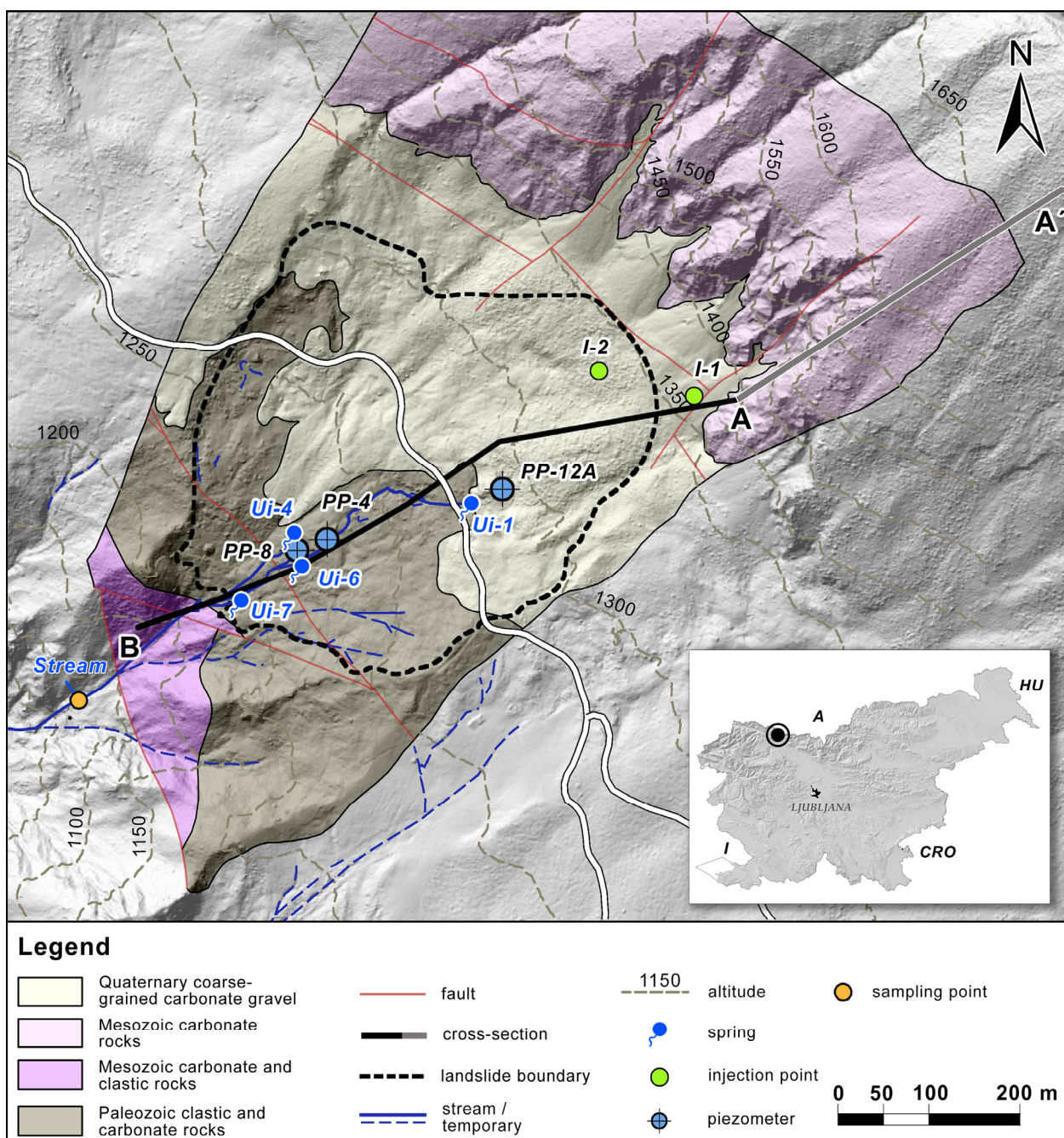


Figure 1. Geological map of the study area with landslide boundary (modified after [26]), tracer injection and sampling points.

3. Materials and Methods

3.1. Groundwater Monitoring

Groundwater temperature and level were measured continuously using two piezometers, PP-8 and PP-12A (Figure 1), equipped with water-level and temperature data loggers (manufactured by the Eltratec (Sveti Jurij ob Ščavnici, Slovenia) and Onset Computer Corporation (Bourne, MA, USA)). The measurements were taken at one-hour intervals.

3.2. Pumping Test

The pumping test in piezometer PP-12A (Figure 1) was conducted on 9 July 2020. We used a 4-inch submersible pump with a maximum pumping capacity of 5 L/s. During the test, the pump intake was positioned at a depth of approximately 17 m. Just above the submersible pump, we installed a probe for the automatic measurement of groundwater level (pressure) and temperature, with a recording interval of 1 s. A pressure probe was also installed simultaneously in the Urbas spring capture, also with a 1 s interval.

3.3. Tracer Tests

When performing the tracing test with sodium chloride, the measuring points were equipped with Eltratec logger, which enables the continuous recording of pressure changes, temperature, and electrical conductivity. The probes were installed in wells and water-courses or springs. For the uranium follow-up test, we used two Cyclops probes to measure fluorescence (Cyclops-7 Loggers, obtained from the American manufacturer Precision Measurement Engineering, Inc., Vista, CA, USA) and one ISCO autosampler, which was used only in the test set of tests. The measurement record for the Cyclops probes was set to a 10 min interval, and the ISCO autosampler was set to take samples every 6 h (four samples per day), which was reduced to every 12 h (two samples per day) in the second half of the test. At other measuring points, samples were taken manually in 250 mL dark bottles and sent to the Karst Research Institute ZRC SAZU, where they were analyzed with a PERKIN ELMER LS 45 luminescent spectrometer (Waltham, MA, USA).

Three series of tracer tests were conducted in the Urbas landslide and its surrounding area: the first in spring 2020, the second in fall 2020, and the final series in spring 2022. The initial tracer test on 17 April 2020 involved dissolving 50 kg of table salt (NaCl) in approximately 200 L of water and injecting the solution near the Ui-1 spring. To monitor the test, probes were installed in observation wells and springs to continuously record electrical conductivity (Table 1). In addition to continuous readings, periodic manual control measurements were performed. The second tracer test was conducted on 14 May 2020. For this test, we injected 2 kg of uranine on the scree slope at location I-1 (Figure 1), just above the landslide scarp. The tracer was diluted with approximately 100 L of water and poured directly into the gravel material. The third tracer test took place on 1 October 2020. We injected uranine below the Urbas spring (Ui-1) at 1:00 p.m. For this test, two sites were equipped with Cyclops automatic fluorometers: borehole PP-8 and the sampling point at the stream (Figure 1). Additionally, samples from each site were collected to determine laboratory fluorescence (Table 1). Concurrently, a fourth tracer test was conducted on 1 October 2020, around 12:00 p.m. A saline solution was injected into borehole PP-12A (Figure 1). Salt was selected as the tracer due to the proximity of the Urbas spring, which supplies drinking water under an allocated water right arrangement. Electrical conductivity measurements were recorded at four monitoring sites: springs Ui-1, Ui-4, and Ui-6, as well as borehole PP-4 (Figure 1). In total, 100 kg of salt was injected into borehole PP-12A and diluted with about 200 L of water. The final series of tests was conducted on 16 May 2022, when we injected 1 kg of uranine solution into the scree slope at injection point I-2 (Figure 1).

For this test, Cyclops loggers were installed at the Ui-1 spring and at a monitoring site at the stream (Figure 1).

Table 1. Main characteristics of tracer experiments.

	Injection Location	Z (m a.s.l.)	Date	Tracer	Tracer Mass (kg)	Sampling Points
1	Ui-1	1270	17 April 2020	NaCl	50	Ui-6, Ui-7, PP-8, PP-4, Urbas stream
2	I-1	1368	14 May 2020	Uranine	2	Ui-1, Urbas stream
3	Ui-1	1270	1 October 2020	Uranine	0.9	Ui-4, Ui-6, Ui-1, PP-4
4	PP-12A	1288	1 October 2020	NaCl	100	Ui-4, Ui-6, Urbas stream, PP-8
5	I-2	1330	16 May 2022	Uranine	1	Ui-1, Ui-4, Urbas stream

4. Results

4.1. Groundwater Monitoring

The fluctuations in groundwater level in both boreholes show similar dynamics. The amplitudes of the fluctuations as well as the depth to the water table are significantly higher in borehole PP-12A, which was located in the upper part of the landslide and covered by a thick layer of coarse-grained gravel (Figure 2). Large fluctuations in groundwater levels in this well indicate the dominant influence of the vigorous flow of groundwater from the upper parts of the landslide recharge area on the groundwater dynamics in this part of the landslide. The constant groundwater temperature indicates deeper and longer groundwater flow paths below the depth at which atmospheric temperature variations and solar radiation exert a clear influence.

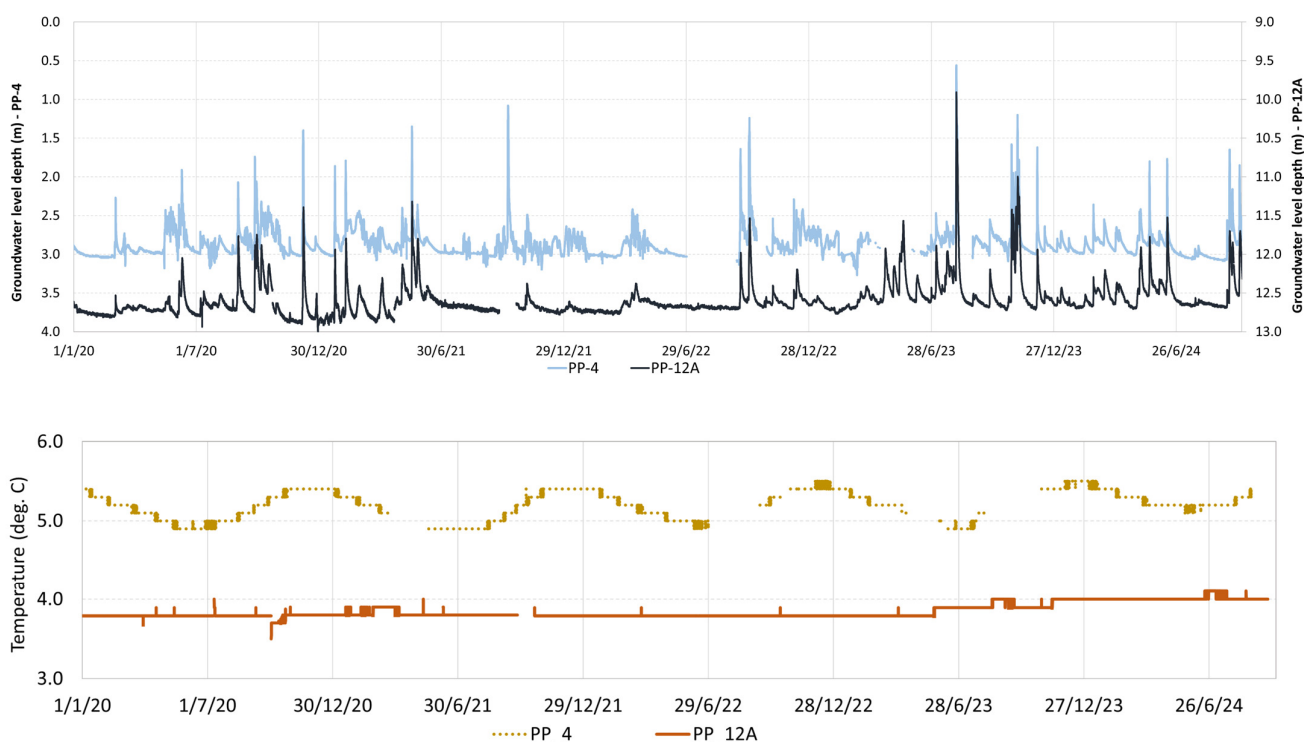


Figure 2. Water-level (above) and temperature (below) fluctuations in piezometers PP-4 and PP-12A.

The smaller fluctuations in the groundwater level and the bigger temperature changes observed in borehole PP-4 indicate shallower groundwater flow in this part of the landslide, which consists of clastic layers of low permeability. Temperature fluctuations in the range of 1.2 °C follow annual cycles with a delay of about half a year compared to fluctuations in air temperature.

4.2. Pumping Test

During the initial pumping, the groundwater level in the well initially declined slowly and steadily. However, after approximately seven minutes, a marked, sudden drop occurred, with the groundwater level decreasing by more than 2 m (Figure 3). This sharp decline, followed by rapid stabilization after approximately 17 min (total drawdown of about 2.6 m), was likely due to the reactivation of the well. The well was drilled in an extremely challenging environment and remained inactive for a considerable period of time after drilling. Therefore, with the start of pumping, we reactivated and flushed the well, effectively cleaning the filter sections. However, the groundwater level continued to drop, eventually reaching the intake basket of the submersible pump, which led to the pump shutting off.

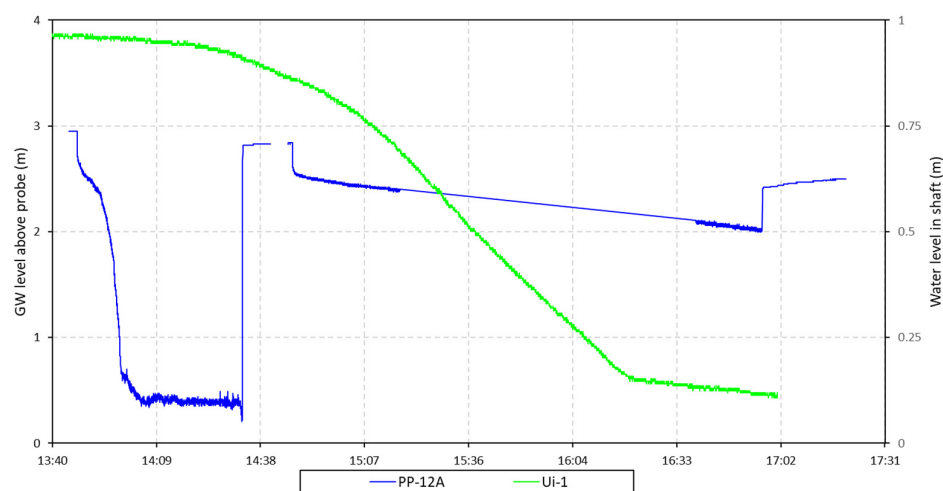


Figure 3. Pumping test results in PP-12A.

The response during the second pumping phase initially mirrored the first prolonged pumping phase. After a gradual and steady initial response, the groundwater level began to drop more intensively about 30 min into pumping and continued to decline steadily over the following two hours until the end of the pumping phase. Following the cessation of pumping, the groundwater level showed a rapid initial rise, which then continued gradually over the course of the following day. Analysis of the drawdown using the Theis method indicated a gravel permeability of $K = 2.24 \times 10^{-3}$ m/s.

During the pumping test, a total of 45 m³ of water was pumped, resulting in a drop in the groundwater level in borehole PP-12A by 0.42 m. Assuming an effective porosity of 20% for the aquifer, we estimate the aquifer area to be around 550 m². Taking other data into account [39], we estimate the aquifer volume in the immediate recharge area of the Urbas spring (Ui-1) at 2026 m³, with a groundwater volume of 405 m³.

4.3. Tracer Tests

4.3.1. Tracer Tests with Salt

First Tracer Test with Salt

At the Ui-6 spring, the electrical conductivity before injection was 250 $\mu\text{S}/\text{cm}$. The first tracer breakthrough was detected at the Ui-6 spring on 18 April 2020, at 16:30, some 26 h and 30 min after injection (Figure 4). The highest electrical conductivity was recorded on 21 April 2020, at 7:45, measuring 327 $\mu\text{S}/\text{cm}$.

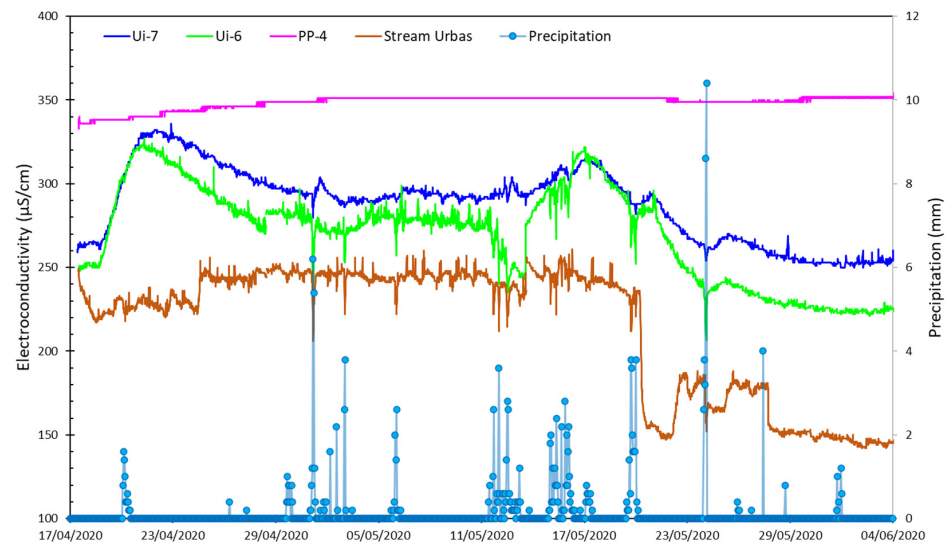


Figure 4. Electroconductivity at sampling points after NaCl injection on 17 April 2020.

At the Ui-7 spring, the electrical conductivity before injection was 265 $\mu\text{S}/\text{cm}$. The first tracer breakthrough was recorded on 18 April 2020, at 20:30, some 30.5 h after injection. The peak tracer concentration was recorded on 21 April 2020, at 21:45, measuring 332 $\mu\text{S}/\text{cm}$. After reaching the peak concentration, the values at the springs began to decline but did not return to pre-injection levels until 23 May 2020. This suggests that the tracer could have lingered at lower concentrations, slowly seeping through the predominantly low-permeability Permo-Carboniferous layers. Water from both springs flows into the Urbas stream, where another monitoring point was set up. No significant changes in the conductivity of the Urbas stream were observed during the tracer test that could be linked to the arrival of the tracer. Minor fluctuations were most likely due to the outflow of various water sources draining into the Urbas stream under different hydrological conditions. The tracer was diluted in the Urbas stream to such an extent that it could not be detected. Similarly, no changes in tracer concentration were observed at the other monitoring points, with any minor changes observed involving a degree of uncertainty.

Second Tracer Test with Salt

On 1 October 2020, around 12:00, we also injected a tracer into borehole PP-12A. However, due to the close proximity of the Urbas spring, which is used as a private drinking water supply, we used salt. Conductivity measurements were carried out at four monitoring locations: the springs Ui-1, Ui-4, and Ui-6, as well as borehole PP-4. We injected 100 kg of salt into borehole PP-12A diluted with approximately 200 L of water. The closest spring to the borehole, located 40 m away, is Ui-1. As expected, the concentration and speed of tracer arrival were the highest at this monitoring location. Conductivity before the injection was 207 $\mu\text{S}/\text{cm}$ (Figure 5). The first elevated conductivity values were detected 4.5 h after injection, with the highest value occurring after 10 h, reaching 379 $\mu\text{S}/\text{cm}$ ($\Delta\text{EC} = 172 \mu\text{S}/\text{cm}$). After reaching its peak, the conductivity steadily

decreased, and after eight days returned to pre-injection levels. Following the Ui-1 spring is borehole PP-4, located some 200 m from the injection point. The increase in conductivity at this monitoring location was the least pronounced, with a rise of just 5 $\mu\text{S}/\text{cm}$ at the highest concentration (338 $\mu\text{S}/\text{cm}$). The highest recorded value of 338 $\mu\text{S}/\text{cm}$ was also the first elevated value we observed after the injection, which occurred 40 h after injection, and remained at this same rate for more than two days.

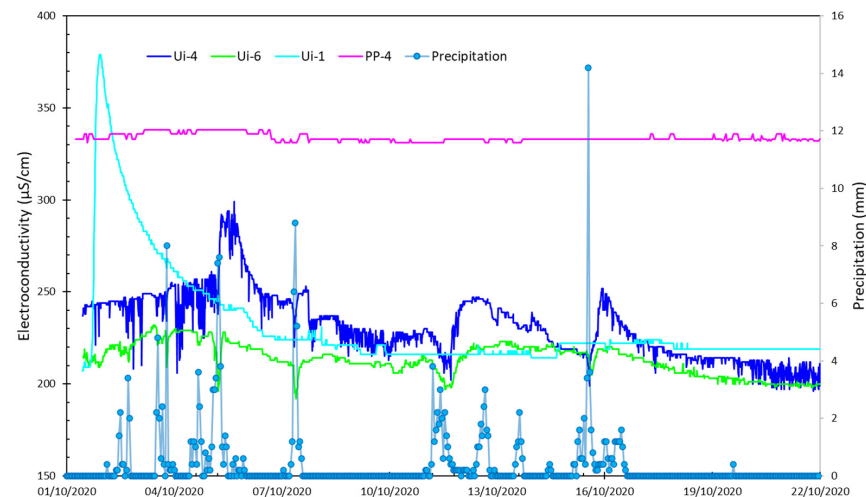


Figure 5. Electroconductivity at sampling points after NaCl injection on 1 October 2020.

More noticeable tracer arrivals were observed at the Ui-4 and Ui-6 springs, which are located at similar distances from borehole PP-12A. At the Ui-4 spring, located 240 m away, conductivity before the injection was 237 $\mu\text{S}/\text{cm}$, with the highest recorded value at 299 $\mu\text{S}/\text{cm}$ ($\Delta\text{EC} = 62 \mu\text{S}/\text{cm}$). The tracer concentration gradually increased from the beginning of the test to its peak, after 100 h. The concentration then decreased for some time and reached significantly elevated levels at least two more times during the test. At the Ui-6 spring, located 250 m from borehole PP-12A, conductivity before the injection was 207 $\mu\text{S}/\text{cm}$, and the highest recorded value was 232 $\mu\text{S}/\text{cm}$ ($\Delta\text{EC} = 25 \mu\text{S}/\text{cm}$). The first elevated tracer concentrations were recorded approximately 12 h after injection, with the highest concentration recorded some 46 h after injection. After reaching its peak, the concentration decreased for some time but, as with the Ui-4 spring, increased significantly at least twice more. In the final phase of the test, the concentration even briefly spiked (248 $\mu\text{S}/\text{cm}$), surpassing the highest value recorded during the initial phase of the test, though the reason for this is unknown.

4.4. Tracer Test with Uranine

4.4.1. First Tracer Test with Uranine (Injection at Scree Slope–14 May 2020)

Based on a preliminary review of cartographic data and known geological and hydro-geological conditions, we selected the injection point for the second test (I-1) on a scree slope, just above the landslide scarp (Figure 1). The injection took place on 14 May 2020, when 2 kg of uranine (a fluorescent dye) was diluted with approximately 100 L of water and poured directly into the gravelly material. Sampling concluded on 10 June 2020. The Urbas stream monitoring site is one of the most important locations, as the stream drains groundwater from the entire Urbas landslide area. Measurements the day after the injection showed minor fluorescence fluctuations, likely due to a rainfall event that increased the stream's turbidity (Figure 6). The first significant increase in concentration was observed on 22 May 2020, at 09:55, with the highest concentration of 0.25 $\mu\text{g}/\text{L}$, which dropped to the baseline the next day. Another brief spike followed shortly after, with a concentration

reaching $0.31 \mu\text{g/L}$ and lasting only 70 min. Two more notable fluorescence increases were recorded on 27 May 2020 and 5 June 2020. The second increase occurred during dry conditions, while the third coincided with an intense rainfall event. In none of these cases did the fluorescence exceed $0.2 \mu\text{g/L}$.

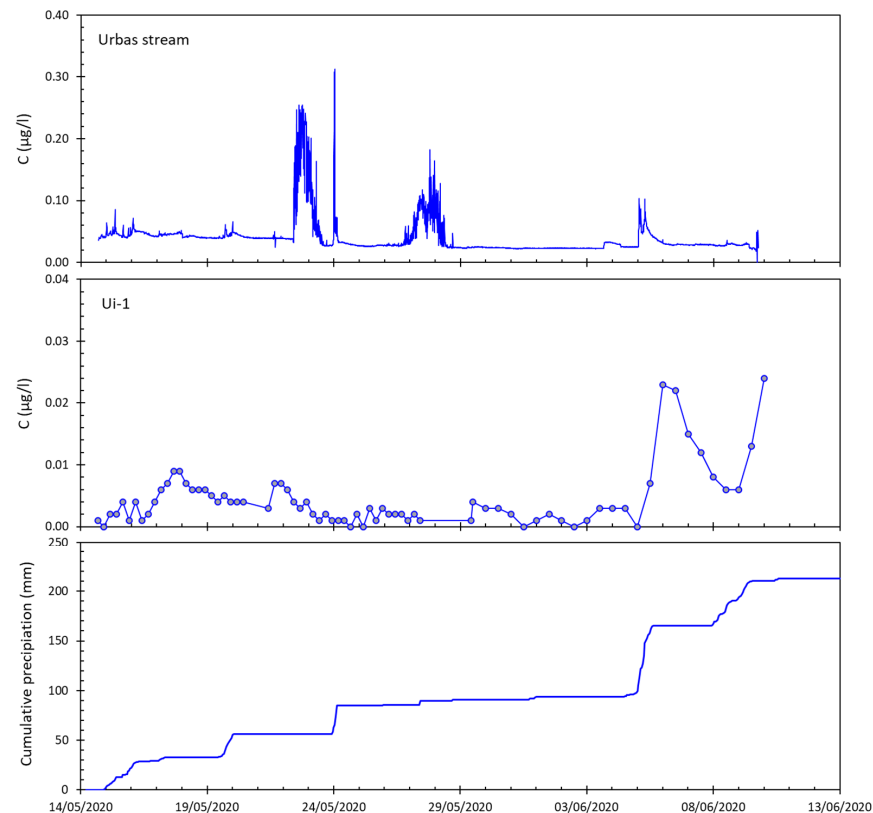


Figure 6. Fluorescence concentrations at sampling points after uranine injection on 14 May 2020.

Continuous measurements were also conducted at the Ui-1 site, the spring closest to the injection point. As shown by the fluorescence fluctuations at the Urbas spring, no tracer breakthrough was detected (Figure 6). Likewise, no tracer was detected at other landslide monitoring sites where manual measurements were taken. The analyzed fluorescence ranges at the monitoring sites were between 0.001 and $0.13 \mu\text{g/L}$. In all cases, the highest fluorescence was recorded at the end of the test, coinciding with intense rainfall, which caused a slight increase in groundwater turbidity (as observed at Ui-1 in Figure 6).

4.4.2. Second Tracer Test with Uranine (Injection at Ui-1–1 October 2020)

During the tracer test on 17 April 2020, no significant increase in conductivity was detected at the Urbas stream monitoring site. It was assumed that this was due to high salt dilution. Therefore, a new tracer test was performed on 1 October 2020, at 13:00, using uranine as the tracer, injected below the Urbas spring. Automatic Cyclops fluorimeters were installed at two locations, the PP-8 borehole and the Urbas stream. For comparison, samples were also collected at both sites for laboratory fluorescence analysis. At borehole PP-8, located approximately 200 m downstream from the injection point, significant differences were observed between continuous fluorimeter measurements and laboratory analyses. Tracer concentrations began to rise on 5 October 2020, at 14:30, 97 h and 30 min after injection (Figure 7). The highest tracer concentration ($206 \mu\text{g/L}$) was recorded on 13 October 2020, at 12:00, 287 h after injection. After reaching the peak concentration, the tracer concentration gradually decreased. Measurements were concluded before the concentration dropped to pre-injection levels due to time constraints. The fluorescence samples, except for the

first, which matched the fluorimeter results, showed a different breakthrough pattern. A significant increase in concentration was already evident in the second sample the day after injection (71.9 $\mu\text{g/L}$). By the third sample, collected on 6 October 2020, the concentration had reached 103.1 $\mu\text{g/L}$, and by 17 October 2020, it had increased slightly to 103.6 $\mu\text{g/L}$. It is worth noting that sampling was conducted using a manual sampler, which remained in the borehole throughout the test to avoid contamination. This sampler allowed for groundwater samples to be taken from a depth of 2 m, the upper part of the water column, while the fluorimeter was installed deeper, in the lower part of the borehole. We suspect that the manual sampling captured the shallow flow zone, while the fluorimeter measured the deeper flow zone, hence the significantly slower breakthrough speeds recorded by the fluorimeter. The most intense inflows into the borehole likely occurred in the lower part, preventing the shallow tracer from mixing within the borehole.

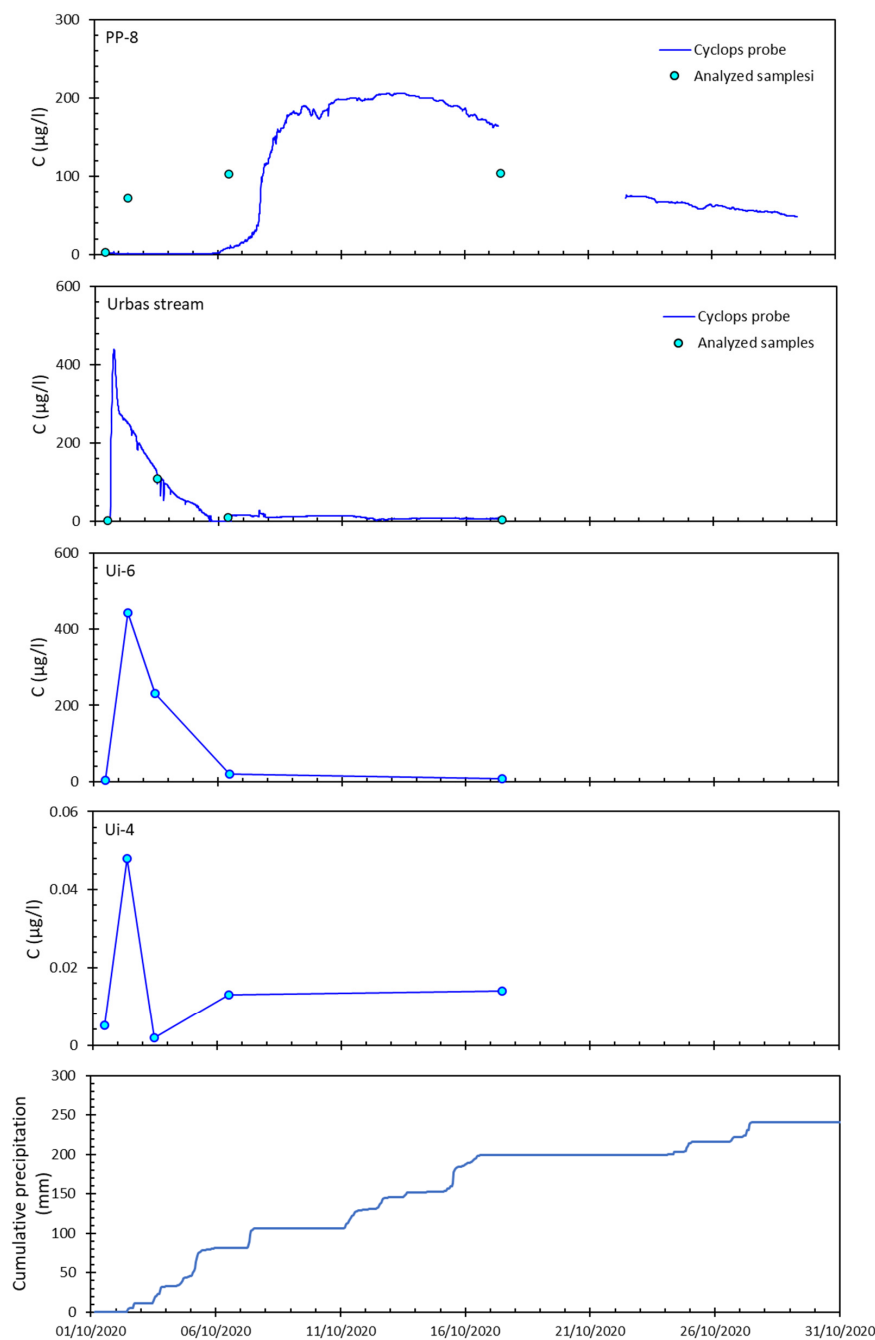


Figure 7. Fluorescence concentrations at sampling points after uranine injection on 1 October 2020.

In the Urbas stream, the breakthrough pattern differed significantly from the PP-4 borehole. As expected, the analyzed samples and fluorimeter measurements matched. Tracer concentrations began to rise sharply after about two hours, with the highest value of 440.4 µg/L reached after 5 h and 20 min. This rapid breakthrough was likely influenced by high water levels and intense surface runoff due to previous rainfall. The concentrations then declined rapidly until 5 October 2020, after which they increased slightly again, matching the measurements from PP-8. The bulk of the tracer thus flowed out before 5 October 2020.

During the test period, additional samples were taken from the Ui-4 and Ui-6 springs. At Ui-6, the highest analyzed concentration was similar to that in the Urbas stream. Since the sample was taken when the concentration was in decline, the peak concentration at this site was likely much higher. Like the Urbas stream, concentrations dropped rapidly after peaking. At the Ui-4 spring, the highest concentration was recorded the day after injection, but it was four orders of magnitude lower than that at Ui-6 (0.05 µg/L). Such concentrations are usually attributed to natural water fluctuations, but since the increased concentration coincided with results at other monitoring sites, we can interpret the tracer’s presence at Ui-4.

4.4.3. Third Tracer Test with Uranine (Injection at Scree Slope–16 May 2022)

The final tracer test was conducted on 16 May 2022 at approximately 14:00, with 1 kg of uranine injected at the scree slope location (injection point I-2, Figure 1). Following the injection, the first traces of the tracer at Ui-1 were detected on 1 August 2022, with a slight increase in concentration (Figure 8). However, a more pronounced rise was observed beginning on 30 August 2022. Estimating the exact time of tracer arrival is challenging due to elevated background concentrations from the previous tracer test in 2020. The highest concentration actually reached was 10.44 µg/L on 12 October 2022.

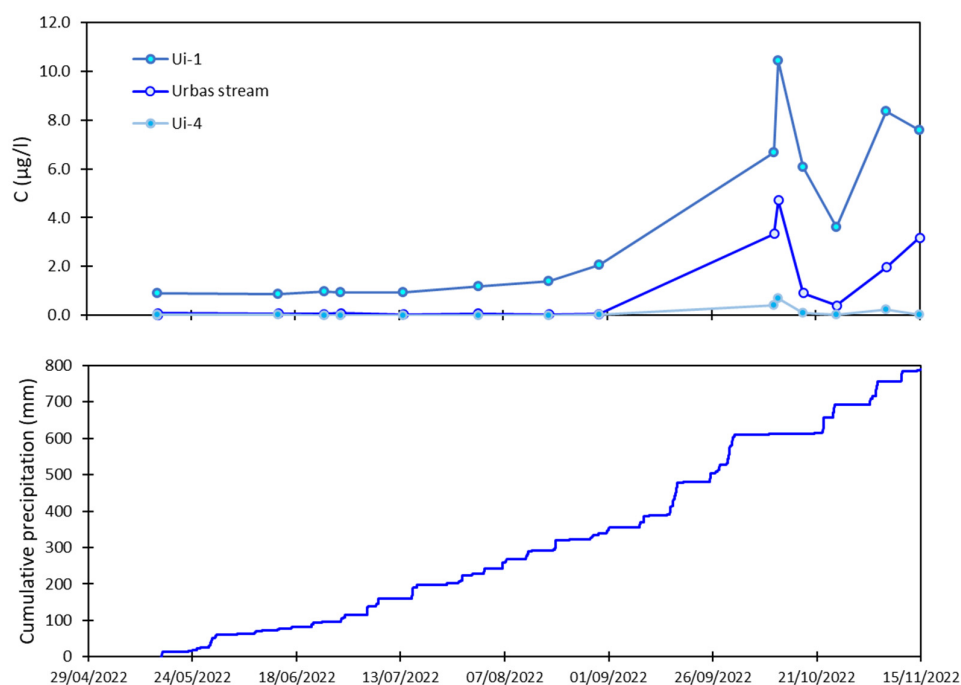


Figure 8. Fluorescence concentrations at sampling points after uranine injection on 16 May 2022.

In the Urbas stream, background concentrations were lower, making it easier to identify the presence of the tracer on 30 August 2022. Sample data from the Urbas stream also showed the highest tracer concentration on 12 October 2022, complicating accurate

determination of the peak. At Ui-4, concentrations remained low, with only occasional sample data available. These samples showed a pattern similar to Ui-1 and the Urbas stream, but with peak concentrations around 0.7 µg/L, which likely represent the presence of the tracer. However, these levels are negligible compared to concentrations observed at Ui-1 and in the Urbas stream.

5. Discussion

The steep gradient of the bedrock surface leads to rapid groundwater drainage, especially during periods of intense precipitation (Figure 9). This results in rapid hydraulic responses, manifested as a rapid increase in spring discharge and a rise in groundwater levels in the landslide body (Figure 2). Both precipitation and inflow from the carbonate hinterland depend on meteorological conditions, making the hydrogeological conditions in the landslide area, and consequently the stability of the landslide, sensitive to variations and seasonal changes in weather patterns. The third tracer test with uranine revealed slower groundwater flow (between 3 and 4 months), which was also indicated by isotope analysis, which estimated an MRT of 0.23 to 0.32 years [30]. The estimated groundwater storage capacity suggests that moisture levels remain elevated even during dry periods, potentially explaining delayed landslide responses to seasonal precipitation trends. Numerical modeling and large-/small-scale model experiments have demonstrated that transient groundwater flow during extreme weather events can create pressure differentials that exacerbate instability [40–43].

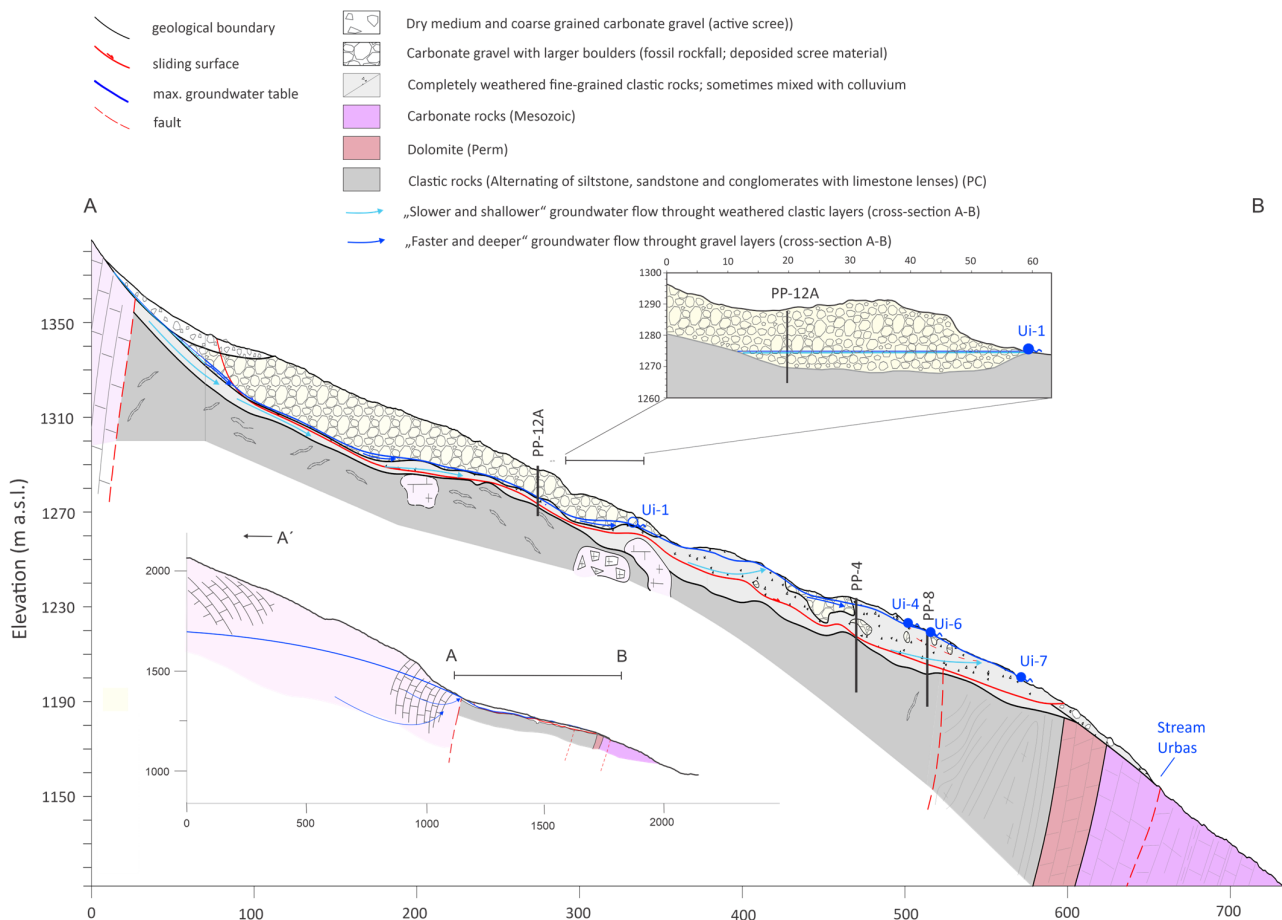


Figure 9. Hydrogeological cross-section A-B with conceptual characteristic groundwater flow within the Urbas landslide (modified after [39]).

The distinction between fast and slow groundwater flow is related to geological conditions. Slower groundwater flow is deeper and is likely to percolate up through the upper, weathered zone of the bedrock. The sliding surface is an additional element that can potentially influence groundwater flow patterns. The deeper flows, although slower, are important for the long-term storage of groundwater and the gradual release of water over longer periods of time. The stable temperature of the groundwater in the aquifer (Figure 2) that recharges the spring confirms this assumption. The groundwater temperature of 4 °C corresponds to the average air temperature in the Julian Alps at an altitude of approx. 1800 m [44], which is consistent with the results of isotopic analyses of previous studies [30], indicating that the water in the springs is recharged from higher altitudes with slower-flowing groundwater.

The Urbas spring is a permanent spring with a stable discharge, which makes it an important source of drinking water. Its stability is ensured by the aquifer above the spring, which allows the temporary storage of groundwater and the recharge of the spring even under very dry conditions. The second salt tracer test confirmed the direct connection between the aquifer and the spring. With the pumping test carried out, we estimated the hydraulic conductivity of the aquifer to be 2.24×10^{-3} m/s.

The stream drains the water from the spring Ui-1 over the landslide. Tracer tests showed that the stream also recharges the groundwater in the landslide body, which is discharged to the surface via the springs in the lower part of the landslide. This process was confirmed by the detection of the tracer in the PP-8 piezometer near the stream and in the springs Ui-7, Ui-6, and Ui-4. However, the stream also functions as a drainage pathway for groundwater in the lower part of the landslide, indicating that the Urbas spring is not the sole outlet for groundwater from the upper landslide recharge area. This was demonstrated in the first uranine tracer test, where the tracer injected at the top of the landslide was detected only in the stream at the lower part of the landslide.

The Urbas landslide area is characterized by geological heterogeneity, which plays an important role in shaping groundwater flow patterns. The combination of highly permeable coarse-grained material and low-permeability clastic material creates a complex system of local aquifers, springs, and groundwater flow paths. This variability affects not only the rate and direction of groundwater movement but also the distribution of water throughout different sections of the landslide. The highly variable permeability within the landslide results in local aquifers that respond rapidly to surface recharge, while deeper, less permeable zones can retain water for longer periods, creating complex groundwater dynamics that are difficult to predict. Tracer-determined groundwater flow velocities therefore indicate a dual-flow system, where fast recharge occurs through preferential pathways, while deeper, slower groundwater flow provides long-term moisture retention in the landslide body. Groundwater infiltration significantly influences pore water pressure, a key factor in landslide movement. A rapid influx of water into the landslide mass due to intense precipitation events can temporarily increase pore pressure, reduce shear strength, and potentially trigger slope displacement. Previous studies have shown that when pore pressure exceeds a critical threshold, landslide acceleration is observed [41,45–47]. In contrast, the slow-moving groundwater component contributes to prolonged saturation of the deeper layers, which can weaken failure surfaces over time, promoting gradual instability.

This complexity poses significant challenges for groundwater management and the planning of measures to improve the stability of the landslide. Interpretation of the hydrogeological conditions, characterized by a combination of fast and slow flow systems, and the highly variable permeability requires a detailed understanding of the local geology and groundwater flow dynamics. Tracer test results can provide valuable supporting information for just such a purpose. Despite the valuable insights provided by tracer tests,

certain limitations must be considered. The use of sodium chloride and fluorescein as tracers may be influenced by factors such as dilution, sorption, and variable flow velocities, which could impact tracer recovery rates and measured travel times [48,49]. Additionally, the spatial resolution of tracer detection is constrained by the number and spatial distribution of monitoring points, potentially overlooking smaller-scale flow heterogeneities [50]. Seasonal variations in groundwater levels and flow rates further complicate tracer interpretations, as different hydrological conditions can affect groundwater flow paths and residence times [51].

The primary causes of the Urbas landslide are linked to its geological composition, hydrogeological conditions, and external triggering factors [52]. The landslide consists of alternating layers of coarse-grained and fine-grained material, allowing rapid infiltration through permeable layers while trapping water in less permeable zones, thereby increasing pore water pressure and reducing slope stability. High seasonal precipitation, combined with snowmelt, results in repeated cycles of saturation and drainage, leading to stress accumulation along failure planes.

Several key factors contribute to the instability of the landslide. Long-term saturation, on the other hand, affects deeper zones, gradually weakening the failure surface and leading to slow deformations. Erosion at the base of the landslide further destabilizes the slope by removing material and reducing support, while seismic activity can induce additional stress along failure planes, increasing the likelihood of movement.

Given the complex hydrogeological conditions characterized by fast and slow flow systems and highly variable permeability, effective landslide management requires a detailed understanding of local geology and groundwater flow dynamics. Tracer test results provide crucial supporting information for this purpose. The relationship between groundwater flow and landslide stability is determined by both the rate of infiltration and the distribution of water storage within the landslide mass. Rapid responses to precipitation events can lead to transient increases in pore water pressure, temporarily reducing shear strength and triggering slope movement [52,53]. In contrast, deeper, slower groundwater flow contributes to long-term stability concerns, as prolonged saturation of deeper layers can weaken critical failure surfaces over time [54]. The estimated hydraulic conductivity values and tracer-determined flow velocities indicate that permeability variations within the landslide create differential pressure zones that may exacerbate instability under extreme weather conditions.

6. Conclusions

The results of this study provide valuable insights into the hydrogeological characteristics and groundwater dynamics of the Urbas landslide area. The groundwater system is influenced by the combination of precipitation infiltration, subsurface inflow from the carbonate recharge area, and the geological heterogeneity of the landslide material. Tracer tests, in combination with groundwater monitoring and pumping tests, reveal a highly complex system of fast, shallow groundwater flows and slower, deep-seated groundwater movement. These results emphasize the importance of both short-term hydrological responses and long-term groundwater storage in shaping landslide stability.

The results show a clear distinction between fast, shallow groundwater flows and slow, deep flow regimes. Shallow flows dominate during and shortly after precipitation events, contributing to rapid responses, such as the emergence of a spring or localized flooding, particularly where permeable gravel layers meet less permeable fine-grained clastic material. In contrast, slower deep flows provide sustained baseflow conditions during dry periods, ensuring long-term water availability. The results of the tracer test

together with isotopic analyses further emphasize the role of the carbonate recharge area in recharging deeper groundwater at higher elevations.

The geological heterogeneity of the Urbas landslide area, characterized by varying permeability and structural complexity, plays an essential role in shaping groundwater flow patterns. This variability results in local aquifers and springs like the major spring Ui-1, as well as smaller springs, such as Ui-4, which respond differently in different hydrological conditions. These dynamics make the groundwater system highly sensitive to short-term hydrological events and at the same time pose a challenge for the prediction of groundwater behavior as well as the effective management of water resources.

The results of this study are of crucial importance for understanding the interplay between groundwater dynamics, geological heterogeneity, and hydrological responses in landslide-prone regions. They emphasize the need for comprehensive groundwater monitoring to effectively manage water resources, manage pollution risks, and assess landslide stability under changing climate and recharge conditions. From a practical perspective, these findings have important implications for groundwater management and landslide hazard mitigation. Understanding the interplay between fast and slow groundwater flow allows for more effective planning of drainage measures and early warning systems. Future efforts should consider both short- and longer-term groundwater dynamics in order to improve hydrological resilience and reduce landslide risks in similar complex terrains.

Author Contributions: Conceptualization, L.S.; methodology, L.S. and M.J.; investigation, L.S. and M.J.; writing—original draft preparation, L.S.; writing—review and editing, M.J.; visualization, L.S.; supervision, M.J.; project administration, M.J.; funding acquisition, M.J. All authors have read and agreed to the published version of the manuscript.

Funding: This study was conducted in the frame of the post-doctoral research project “Regional groundwater flow dynamics in alpine carbonate aquifers: mechanisms, boundary conditions and the impact of climate change” (Z1-50031) and the research program Groundwater and Geochemistry (P1-0020), both funded by the Slovenian Research and Innovation Agency (ARIS). Additional financial support was provided by the Ministry of Environment and Spatial Planning of the Republic of Slovenia.

Institutional Review Board Statement: Not applicable.

Informed Consent Statement: Not applicable.

Data Availability Statement: The raw data supporting the conclusions of this article will be made available by the authors on request.

Conflicts of Interest: The authors declare no conflicts of interest.

References

1. Van Asch, T.W.J.; Buma, J.; Van Beek, L.P.H. A view on some hydrological triggering systems in landslides. *Geomorphology* **1999**, *30*, 25–32. [[CrossRef](#)]
2. Iverson, R.M. Landslide triggering by rain infiltration. *Water Resour. Res.* **2000**, *36*, 1897–1910. [[CrossRef](#)]
3. Lambe, W.T.; Whitman, R.V. *Soil Mechanics, SI version*; J. Wiley and Sons: New York, NY, USA, 1979.
4. Rutqvist, J.; Stephansson, O. The role of hydromechanical coupling in fractured rock engineering. *Hydrogeol. J.* **2003**, *11*, 7–40. [[CrossRef](#)]
5. Schneider, P.; Pool, S.; Strouhal, L.; Seibert, J. True colors—Experimental identification of hydrological processes at a hillslope prone to slide. *Hydrol. Earth Syst. Sci.* **2014**, *18*, 875–892. [[CrossRef](#)]
6. Hought, D.R.W.; Tromp-van Meerveld, I. Spatial variation in transient water table responses: Differences between an upper and lower hillslope zone. *Hydrol. Process.* **2011**, *25*, 3866–3877. [[CrossRef](#)]
7. Onda, Y.; Komatsu, Y.; Tsujimura, M.; Fujihara, J. The role of subsurface runoff through bedrock on storm flow generation. *Hydrol. Process.* **2001**, *15*, 1693–1706. [[CrossRef](#)]

8. Uchida, T.; Kosugi, K.; Mizuyama, T. Effects of pipe flow and bedrock groundwater on runoff generation in a steep headwater catchment in Ashiu, central Japan. *Water Resour. Res.* **2002**, *38*, 715–724. [[CrossRef](#)]
9. Uchida, T.; Tromp-van Meerveld, I.; McDonnell, J.J. The role of lateral pipe flow in hillslope runoff response: An intercomparison of non-linear hillslope response. *J. Hydrol.* **2005**, *311*, 117–133. [[CrossRef](#)]
10. Tromp-van Meerveld, I.; Weiler, M. Hillslope dynamics modeled with increasing complexity. *J. Hydrol.* **2008**, *361*, 24–40. [[CrossRef](#)]
11. Cao, V.; Schaffer, M.; Taherdangkoo, R.; Licha, T. Solute Reactive Tracers for Hydrogeological Applications: A Short Review and Future Prospects. *Water* **2020**, *12*, 653. [[CrossRef](#)]
12. Goldscheider, N.; Meiman, J.; Pronk, M.; Smart, C. Tracer tests in karst hydrogeology and speleology. *Int. J. Speleol.* **2008**, *37*, 27–40. [[CrossRef](#)]
13. Petrič, M. Review of water tracing with artificial tracers on karst areas in Slovenia. *Geologija* **2009**, *52*, 127–136. [[CrossRef](#)]
14. Petrič, M. The Use of Artificial Tracer Tests in the Process of Management of Karst Water Resources in Slovenia. In *Karst Water Environment. The Handbook of Environmental Chemistry*; Younos, T., Schreiber, M., Kosič Ficco, K., Eds.; Springer: Cham, Switzerland, 2019; p. 68. [[CrossRef](#)]
15. Lauber, U.; Goldscheider, N. Use of artificial and natural tracers to assess groundwater transit-time distribution and flow systems in a high-alpine karst system (Wetterstein Mountains, Germany). *Hydrogeol. J.* **2014**, *22*, 1807. [[CrossRef](#)]
16. Benischke, R. Advances in the methodology and application of tracing in karst aquifers. *Hydrogeol. J.* **2021**, *29*, 67–88. [[CrossRef](#)]
17. Ronchetti, F.; Piccinini, L.; Deiana, M.; Ciccacese, G.; Vincenzi, V.; Aguzzoli, A.; Malavasi, G.; Fabbri, P.; Corsini, A. Tracer test to assess flow and transport parameters of an earth slide: The Montecagno landslide case study (Italy). *Eng. Geol.* **2020**, *275*, 105749. [[CrossRef](#)]
18. Debieche, T.H.; Bogaard, T.A.; Marc, V.; Emblanch, C.; Krzeminska, D.M.; Malet, J.P. Hydrological and hydrochemical processes observed during a large-scale infiltration experiment at the Super-Sauze mudslide (France). *Hydrol. Process.* **2012**, *26*, 2157–2170. [[CrossRef](#)]
19. Charlier, J.B.; Bertrand, C.; Binet, S.; Mudry, J.; Bouillier, N. Use of continuous measurements of dissolved organic matter fluorescence in groundwater to characterize fast infiltration through an unstable fractured hillslope (Valabres rockfall, French Alps). *Hydrogeol. J.* **2010**, *18*, 1963–1969. [[CrossRef](#)]
20. Frei, C.; Herfort, M.; Loew, S.; Leuenberger-West, F. First results of a large-scale multi-tracer test within an unstable rockslide area (Åknes, Norway). *Geophys. Res. Abstr.* **2008**, *10*.
21. Gargini, A.; De Nardo, M.T.; Piccinini, L.; Segadelli, S.; Vincenzi, V. Spring discharge and groundwater flow systems in sedimentary and ophiolitic hard rock aquifers: Experiences from Northern Apennines (Italy). In *Fractured Rock Hydrogeology*; Sharp, J.M., Ed.; CRC Press: Boca Raton, FL, USA, 2014; pp. 129–146.
22. Vallet, A.; Bertrand, C.; Mudry, J.; Bogaard, T.; Fabbri, O.; Baudement, C.; Régent, B. Contribution of time-related environmental tracing combined with tracer tests for characterization of a groundwater conceptual model: A case study at the Séchilienne landslide, western Alps (France). *Hydrogeol. J.* **2015**, *23*, 1761–1779. [[CrossRef](#)]
23. Crosta, G.B.; Di Prisco, C.; Frattini, P.; Frigerio, G.; Castellanza, R.; Agliardi, F. Chasing a complete understanding of the triggering mechanisms of a large rapidly evolving rockslide. *Landslides* **2014**, *11*, 747–764. [[CrossRef](#)]
24. Delle Piane, L.; Perello, P.; Baietto, A.; Giorza, A.; Musso, A.; Gabriele, P.; Baster, I. Mature vs. active deep-seated landslides: A comparison through two case histories in the Alps. *Rock. Mech. Rock. Eng.* **2016**, *49*, 2189–2216. [[CrossRef](#)]
25. Janža, M.; Serianz, L.; Šram, D.; Klasinc, M. Hydrogeological investigation of landslides Urbas and Čikla above the settlement of Koroška Bela (NW Slovenia). *Geologija* **2018**, *61*, 191–203. [[CrossRef](#)]
26. Peternel, T.; Jež, J.; Milanič, B.; Markelj, A.; Jemec Auflič, M. Engineering-geological conditions of landslides above the settlement of Koroška Bela (NW Slovenia). *Geologija* **2018**, *61*, 177–189. [[CrossRef](#)]
27. Bezak, N.; Sodnik, J.; Maček, M.; Jurček, T.; Jež, J.; Peternel, T.; Mikoš, M. Investigation of potential debris flows above the Koroška Bela settlement, NW Slovenia, from hydro-technical and conceptual design perspectives. *Landslides* **2021**, *18*, 3891–3906. [[CrossRef](#)]
28. Šegina, E.; Peternel, T.; Urbančič, T.; Realini, E.; Zupan, M.; Jež, J.; Caldera, S.; Gatti, A.; Tagliaferro, G.; Consoli, A.; et al. Monitoring Surface Displacement of a Deep-Seated Landslide by a Low-Cost and near Real-Time GNSS System. *Remote Sens.* **2020**, *12*, 3375. [[CrossRef](#)]
29. Peternel, T.; Šegina, E.; Zupan, M.; Jemec Auflič, M.; Jež, J. Preliminary Result of Real-Time Landslide Monitoring in the Case of the Hinterland of Koroška Bela, NW Slovenia. In *Understanding and Reducing Landslide Disaster Risk*; Springer International Publishing: Berlin/Heidelberg, Germany, 2021; pp. 459–464.
30. Koren, K.; Serianz, L.; Janža, M. Characterizing the Groundwater Flow Regime in a Landslide Recharge Area Using Stable Isotopes: A Case Study of the Urbas Landslide Area in NW Slovenia. *Water* **2022**, *14*, 912. [[CrossRef](#)]
31. Leibundgut, C.; Maloszewski, P.; Külls, C. *Tracers in Hydrology*; Wiley: New York, NY, USA, 2011; 432p.
32. Jemec Auflič, M.; Mikoš, M.; Verbovšek, T. Advances in Landslide Research. In Proceedings of the 3rd Regional Symposium on Landslides in the Adriatic Balcan Region, Ljubljana, Slovenia, 11–13 October 2017.

33. Jež, J.; Mikoš, M.; Trajanova, M.; Kumelj, Š.; Budkovič, T.; Bavec, M. Koroška Bela alluvial fan—The result of the catastrophic slope events; Karavanke Mountains, NW Slovenia). *Geologija* **2008**, *51*, 219–227. [[CrossRef](#)]
34. SEA. Annual Data (1981–2019) at Javorniški Rovt. 2024. Available online: <http://meteo.arso.gov.si/met/sl/app/webmet/#webmet==8Sdwx2bhR2cv0WZ0V2bvEGcw9ydlJWblR3LwVnaz9SYtVmYh9icdFGbt9SaulGdugXbsx3cs9mdl5WahxXYyNGapZXZ8tHZv1WYp5mOnMHbvZXZulWYnwCchJXYtVGdlJnOn0UQQdSf> (accessed on 20 November 2024).
35. Črepinšek, Z.; Kunšič, A.; Kralj, T.; Kajfež-Bogataj, L. Precipitation analysis of the wider area of the Triglav national park for the period 1961–2009. *Acta Agric. Slov.* **2011**, *97*, 295–304.
36. Kunšič, A. Precipitation Analysis of the Wider Area of the Triglav National Park. Bachelor Thesis, University of Ljubljana, Ljubljana, Slovenia, 2011.
37. SEA. Environmental Atlas of Slovenia. 2024. Available online: http://gis.arso.gov.si/atlasokolja/profile.aspx?id=Atlas_Okolja_AXL@ARSO&culture=en-US (accessed on 10 January 2024).
38. Šegina, E.; Jemec Auflič, M.; Zupan, M.; Jež, J.; Peternel, T. Composite landslide in the dynamic alpine conditions: A case study of Urbas landslide. *Geologija* **2022**, *65*, 161–175. [[CrossRef](#)]
39. Peternel, T.; Jež, J.; Janža, M.; Zupan, M.; Markelj, A.; Maček, M.; Logar, J.; Smolar, J.; Mikoš, M.; Bezak, N.; et al. *Podrobna Geološka-Geotehnična in Hidrogeološka Karakterizacija Velikih Plazov v Zaledju Naselja Koroška Bela za Potrebe Izdelave Stabilnostnih Analiz in Študijo Izvedljivosti Sanacijskih Rešitev: Krovno Poročilo*; Geološki Zavod Slovenije, Fakulteta za Gradbeništvo in Geodezijo: Ljubljana, Slovenia, 2020; p. 218.
40. Lu, N.; Godt, J.W. *Hillslope Hydrology and Stability*; Cambridge University Press: Cambridge, UK, 2013. [[CrossRef](#)]
41. Wang, G.; Sassa, K. Factors affecting rainfall-induced flowslides in laboratory flume tests. *Géotechnique* **2001**, *51*, 587–599. [[CrossRef](#)]
42. Cai, F.; Ugai, K. Numerical analysis of rainfall effects on slope stability. *Int. J. Geomech.* **2004**, *4*, 69–78. [[CrossRef](#)]
43. Tian, D.; Zhen, H.; Liu, D. A 2D integrated FEM model for surfacewater–groundwater flow of slopes under rainfall condition. *Landslides* **2017**, *14*, 577–593. [[CrossRef](#)]
44. Serianz, L. Hidrogeološka Analiza Vodne Bilance Reke Radovne: Hydrogeological Analysis of River Radovna Water Balance. Master’s Thesis, University of Ljubljana, Ljubljana, Slovenia, 2015.
45. Iverson, R.M.; Reid, M.E.; Iverson, N.R.; LaHusen, R.G.; Logan, M.; Mann, J.E.; Brien, D.L. Acute sensitivity of landslide rates to initial soil porosity. *Science* **2000**, *290*, 513–516. [[CrossRef](#)] [[PubMed](#)]
46. Iverson, R.M. Regulation of landslide motion by dilatancy and pore pressure feedback. *J. Geophys. Res. Earth Surf.* **2005**, *110*, F02015. [[CrossRef](#)]
47. Schulz, W.H.; McKenna, J.P.; Kibler, J.D.; Biavati, G. Relations between hydrology and velocity of a continuously moving landslide—Evidence of pore-pressure feedback regulating landslide motion? *Landslides* **2009**, *6*, 181–190. [[CrossRef](#)]
48. Leibundgut, A.C.; Maloszewski, P.; Külls, C.; Leibundgut, C.; Maloszewski, P. *Tracers in Hydrology*; John Wiley & Sons, Ltd.: Chichester, UK, 2009; 432p.
49. Käss, W. *Tracing Technique in Geohydrology*; Balkema: Rotterdam, The Netherlands, 1999; 602p. [[CrossRef](#)]
50. Goldscheider, N.; Drew, D. *Methods in Karst Hydrogeology*; Taylor & Francis: Abingdon, UK, 2007; 280p. [[CrossRef](#)]
51. Ford, D.; Williams, P. *Karst Hydrogeology and Geomorphology*; Wiley: Hoboken, NJ, USA, 2007. [[CrossRef](#)]
52. Peternel, T.; Janža, M.; Šegina, E.; Bezak, N.; Maček, M. Recognition of Landslide Triggering Mechanisms and Dynamics Using GNSS, UAV Photogrammetry and In Situ Monitoring Data. *Remote Sens.* **2022**, *14*, 3277. [[CrossRef](#)]
53. Bogaard, T.A.; Greco, R. Landslide hydrology: From hydrology to pore pressure. *Earth-Sci. Rev.* **2018**, *185*, 120–150. [[CrossRef](#)]
54. Moser, M.; Hohensinn, F. Geotechnical aspects of soil slips in Alpine regions. *Eng. Geol.* **1983**, *19*, 185–211. [[CrossRef](#)]

Disclaimer/Publisher’s Note: The statements, opinions and data contained in all publications are solely those of the individual author(s) and contributor(s) and not of MDPI and/or the editor(s). MDPI and/or the editor(s) disclaim responsibility for any injury to people or property resulting from any ideas, methods, instructions or products referred to in the content.